

Trajectory Optimization for Thermally-Actuated Soft Planar Robot Limbs

Anthony Wertz^{1*}, Andrew P. Sabelhaus^{2*}, Carmel Majidi^{1,2}

Abstract—Practical use of robotic manipulators made from soft materials will require planning for complex motions. We present the first approach for generating trajectories of a thermally-actuated soft robotic manipulator. Based on simplified approximations of the soft arm and its shape-memory-alloy (SMA) wires, we justify a dynamics model of a discretized rigid manipulator with joint torques proportional to wire temperature. Then, we propose a method to calibrate this model from hardware data, and demonstrate that the simulation aligns well with a test trajectory. Finally, we use direct collocation trajectory optimization with the non-linear dynamics to derive open-loop controls for feasible trajectories that closely align with desired reference inputs. Two example trajectories are verified in hardware. The results show promise for both open-loop planning as well as for future applications with feedback.

I. INTRODUCTION

Robotic systems composed of soft materials have the potential to outperform rigid robots in tasks that require biomimetic deformability and safe and robust interactions with their surroundings [1], [2]. Putting these robots to practical use, however, requires performing complex planned motions that are similar to those performed with rigid robots. At the moment, many soft robots are simplistic in the actions they take and are incapable of matching the complex motion trajectories that can be achieved with rigid robots. This is due to limitations in actuation and design [3] as well as modeling [4] for very high-degree-of-freedom state spaces. Determining what actions may be possible for a soft robot, as well as how to execute them, requires models that are both computationally tractable yet match hardware. This is particularly challenging with soft robots that are actuated using thermally-responsive materials such as shape memory alloy (SMA), which have become increasingly popular within the field [5], [6], [7]. Because of transient temperature effects, such thermal actuators are especially difficult to model and simulate [8] for applications in soft robotics.

This article proposes a framework for modeling and trajectory optimization of soft robotic limbs actuated with antagonistic thermal actuators (Fig. 1). Relying both on prior

work alongside approximations from first-principle models, we develop a three-part dynamics model based on a discretized rigid manipulator, a conversion from actuator temperature to discretized joint torques, and Joule heating. We construct a hardware prototype of a soft-limb robot with two shape-memory alloy (SMA) actuators, motivated by [9], now including temperature and displacement sensing. We provide a methodology to calibrate our model from hardware data. Then, we develop a direct collocation approach to optimize motion trajectories of this limb. Open-loop tests of these trajectories show that the result aligns well with hardware.

The method proposed here focuses on the trajectory optimization problem, as opposed to closed loop control. Feedback has been extensively studied for thermal and shape-memory actuators in soft robots [10], [11], [12] as well as soft robots with controllable-force actuators (i.e., pneumatics) [13], [14]. Trajectory optimization offers two distinct benefits in comparison to feedback without pre-planned trajectories [15]. First, an optimized trajectory verifies dynamic feasibility of a motion a-priori, a common requirement and significant challenge for many state-feedback techniques (such as model-predictive control [16]) in soft and flexible robots. Second, trajectory optimization allows for creating feasible trajectories for different goals: for example, minimum energy expenditure versus minimum time [15]. Since thermal actuators have significant energy requirements [3], these are often opposing goals.

This article is the first to introduce an approach to trajectory optimization of soft manipulators with thermal (and shape memory) actuators. We demonstrate that commonly-used robotics models translate well to this problem, trading-off the accuracy of computationally-intensive soft dynamics [17] in favor of a practical solution. Though we demonstrate our result using only a single segment of a soft limb with two actuators, we expect that the approach will adapt to multi-limb robots given the structure of the underlying dynamics equations.

II. RELATED WORK

This article considers soft limbs actuated with shape-memory-alloy wires and polymers, which have size and work density benefits [18] over more common soft actuation strategies such as pneumatics and cable drive [19], and are therefore promising for compact untethered soft robots [9]. However, both pneumatic/hydraulic actuation and cable-driven soft robots can assume that a controller specifies a force, as occurs with motors on rigid robots [13], [20], [21],

This work was in part supported by the Office of Naval Research under Grant No. N000141712063 (PM: Dr. Tom McKenna), the National Oceanographic Partnership Program (NOPP) under Grant No. N000141812843 (PM: Dr. Reginald Beach), and an Intelligence Community Postdoctoral Research Fellowship through the Oak Ridge Institute for Science and Education.

¹A. Wertz and C. Majidi are with the Robotics Institute, Carnegie Mellon University, Pittsburgh PA, USA. awertz, cmajidi@andrew.cmu.edu

²A.P. Sabelhaus and C. Majidi are with the Department of Mechanical Engineering, Carnegie Mellon University, Pittsburgh PA, USA. apsabelhaus@cmu.edu

*A. Wertz and A.P. Sabelhaus contributed equally to this work.

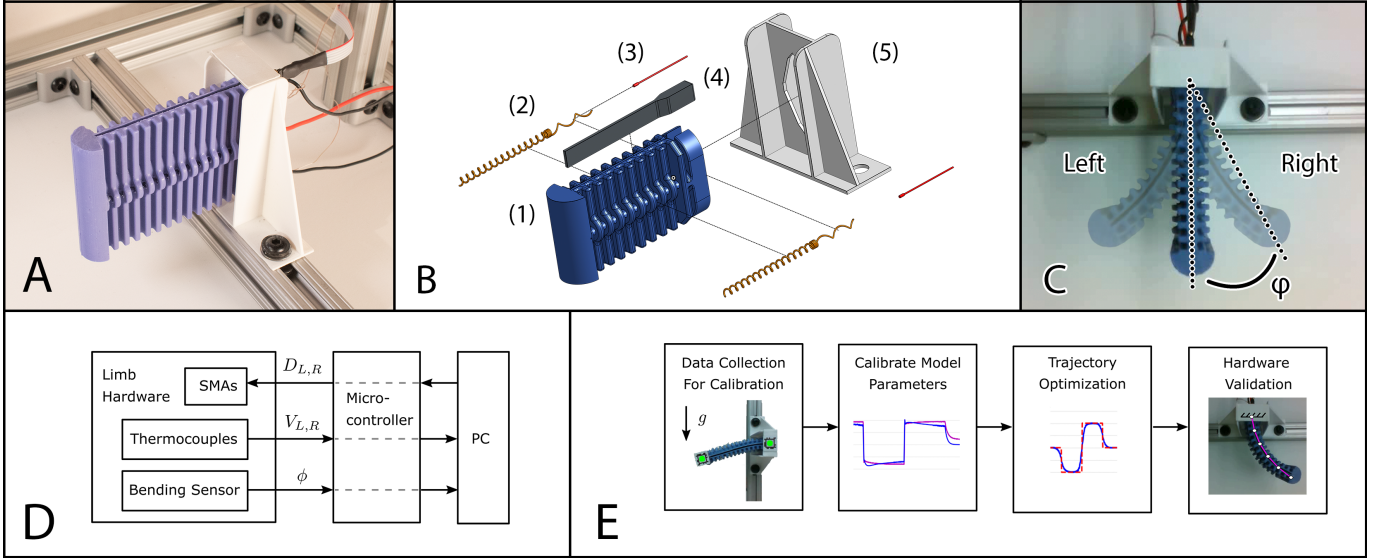


Fig. 1: Hardware, test setup, and operation of the soft SMA-actuated limb. The limb (A) consists of cast bulk silicone (B1) actuated by two antagonistic SMA coils attached along either transverse side (B2). It contains thermocouples for temperature measurements of each SMA (B3) and a sensor for bending angle (B4). A bracket (B5) holds the limb vertically, so that it experiences no gravitational forces. The limb’s SMA coils are actuated via Joule heating, producing bending motions (C) via a pulse width modulation (PWM) signal from a microcontroller (D). Our overall procedure (E) consists of hardware data collection under specific conditions to calibrate the parameters of the model, then we perform a direct collocation optimization for feasible trajectories, which are finally verified in hardware.

whereas control of force in thermal actuation only occurs indirectly [22].

For these robots, since out-of-the-box robotics models fail to capture these actuator dynamics, little work has developed state-space trajectory generation or optimization. Prior work includes A* to optimize an SMA array [23] and evolutionary algorithms to for trajectory optimization of antagonistic SMA actuators [24]. However, neither example translates those results to hardware, nor is there much focus on or results for open-loop tracking. There have been attempts at open-loop task-space operation [25], though none has taken this as an explicit focus.

Many different models for the kinematics and dynamics of soft-bodied robot arms are available to use for our goal [26] with varying trade-offs between complexity and computational requirements versus physical accuracy. More physically-accurate models include the discrete elastic rod (DER) [27], [28], [17]. Kinematics and dynamics that are more computationally-tractable, and useful for state-space representations, include the constant-curvature framework in particular [29], [14]. These may all be used in future work in combination with our actuator dynamics. We choose, however, to use one of the simplest possible representations, a discretized rigid manipulator, motivated by approximations of the above alongside promising contemporary results [20].

Accurate dynamics for thermal actuators is often based on first principles and constitutive models [30], [18]. However, these often require measurements of stress in addition to strain [8], a challenging task for robotic design. These examples did not combine with a soft-body dynamics model, and the many

coupled states make optimization a challenge. However, the commonality among many of these is the temperature change itself, often expressed as Joule/resistive heating alongside passive convective cooling [31], [22]. This article therefore considers if temperature alone can approximate a more complicated stress/strain actuator response.

III. HARDWARE PLATFORM

Our soft limb (Fig. 1A,B) is derived from prior work in a legged robot [9], with the intent to eventually be employed in that setting. The limb body was cast from bulk silicone elastomer (Smooth-Sil 960, Smooth-On) and embedded with nickel-titanium alloy (nitinol) SMA actuator coils (Flexinol, Dynalloy), a capacitive bend sensor (single axis, Bend Labs), and power cables. Chromel–alumel (K-type) thermocouples (Digilent, Inc.) for measuring wire temperature were bonded to the bracketed side of the SMA actuators with thermally conductive, electrically insulating epoxy (MG 8329TCF). The limb was mounted with a 3D-printed bracket oriented with the bending axis antiparallel to gravity (figure 1) so the gravitational loading can be ignored.

Sensor measurement and control was achieved through a development board with an ARM processor (nRF52-DK, Nordic Semiconductor). The thermocouples interfaced a MAX31855 integrated circuit for cold-junction compensation and signal amplification, which subsequently communicated with the microcontroller over the Serial Peripheral Interface (SPI) bus. The bend sensor communicated directly to the microcontroller over the Inter-Integrated Circuit (I2C) bus. Pulse-width modulation was used as the gate input on N-

channel power MOSFETs to modulate current through the thermal actuators.

IV. DYNAMICS MODELING

The approach in this article makes approximations to each of the three relevant dynamics phenomena of our robot limb: the manipulator body, the discretized joint torques, and the actuator temperature. These are combined into a final set of equations of motion, taking a pulse-width modulation (PWM) voltage on the SMA wires as input and predicting the manipulator's bending angle as output.

A. Rigid manipulator model

This article employs a simplified model of a discretized rigid manipulator for the robot's body. Two observations motivate this approach. First, we note that recent work has demonstrated relatively accurate simulations of soft fluid-driven limbs as discretized manipulators [20]. Second, we note that the discrete elastic rod (DER) model of SMA-powered soft robots [28], [17], which has been previously validated for in hardware, has its energy expressed in terms of linear and angular displacements - similar to the prismatic and rotational joints of a robot arm. Noting that our robot shows no meaningful centerline extension, the DER becomes a discretized elastica - i.e., with fixed "joint lengths" between discretization points.

The remaining energetic contribution to the rod dynamics is bending energy at each discretization point, $E_b^i = \frac{1}{2}\alpha(\kappa_i - \bar{\kappa}_i)^2$, where α is a constant and $\kappa_i(\theta_i)$ is a nonlinear function of the angle between segments. Approximating bending energy instead as a *linear* function of angle reduces down to linear torsional springs at each discretization point. The result is a serial-chain rigid manipulator with flexible joints at each point (Fig. 2), with mass matrix M , Coriolis and centrifugal terms C , and spring constant k :

$$M(\theta)\ddot{\theta} + C(\theta, \dot{\theta})\dot{\theta} + k(\theta - \bar{\theta}) + \sigma\dot{\theta} = 0, \quad (1)$$

where linear damping is added for energy dissipation in the soft material, as in [17], and θ is a vector of angles between the n discretized segments: $\theta = [\theta_1, \theta_2, \dots, \theta_n]$, hereafter referred to as joint angles.

From the work in [17], rods actuated by SMAs can be modeled as a changing set-point angle of the torsional energy at each joint, i.e., actuation occurs as $\bar{\theta}$ changes. We assume this occurs as a function of temperature in our two SMAs, T_l and T_r . Refactoring eqn. (1) by noting that k distributes through our linear spring, our equations of motion are

$$M(\theta)\ddot{\theta} + C(\theta, \dot{\theta})\dot{\theta} + k\theta + \sigma\dot{\theta} = \tau, \quad (2)$$

$$\tau = k\bar{\theta}(T_l, T_r).$$

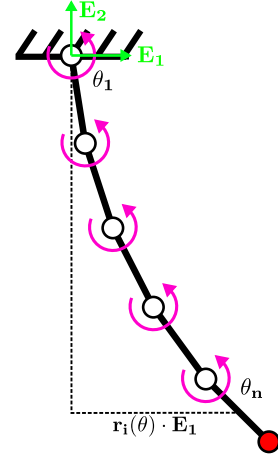


Fig. 2: The limb is modeled as a five link rigid manipulator with uniformly spaced revolute joints rotating normal to the plane. The joints are indexed one through n starting from the base. The base joint cannot translate but is free to rotate. The origin is centered on the first joint. Link center of mass offset $r_i(\theta) \cdot E_1$ is used in computing the spring constant in eqn. 7.

B. SMA actuator model

The model in eqn. (2) requires a mapping $\bar{\theta}(T_l, T_r)$ between wire temperature and our discretized joint torque, as well as temperature as a function of input energy. This formulation neglects the internal constitutive properties of the SMA wire, assuming that resulting torques are only a function of temperature. For each of the two actuators, the SMA temperature dynamics are modeled using an extension of the simple Joule heating model proposed in [22]:

$$C_v \dot{T} = -h_c A_c (T - T_{amb}) + \rho J^2 D$$

$$= a_1 (T - T_{amb}) + a_2 D$$

with specific heat capacity C_v ; ambient heat convection coefficient h_c ; convective surface area A_c ; ambient temperature T_{amb} ; current density J modulated by the control duty cycle D ; and wire resistance ρ . To simplify the expression the parameters were lumped together, yielding $a_1 = -h_c A_c / C_v$ and $a_2 = \rho J^2 / C_v$.

It is important to note that the embedded thermocouple is not in direct contact with the SMA wire and can not be used to directly measure the wire temperature. To make a robust connection between the thermocouple and the SMA wire we bonded it using a small amount of thermally conductive, electrically insulating epoxy. This adds thermal mass that heats and cools more slowly than the wire itself, so we added a coupled equation that represents the temperature change in the epoxy. The measured temperature V is assumed to heat up and cool down delayed slightly to the true SMA temperature, and the coefficient a_3 is used to model its time response. This forms the following system of differential equations:

$$\dot{T} = a_1(T - T_{amb}) + a_2 D, \quad (3)$$

$$\dot{V} = a_3(V - T), \quad (4)$$

where V is the measured temperature of the epoxy in contact with the thermocouple, and a_3 is formed again by lumping the parameters. In this model we treated all parameters as constant and we do not take into account the martensite fraction.

To map the temperature dynamics to discretized joint torques we consider the constitutive model for SMA strain. From [30]:

$$\tau - \tau_0 = G(\xi)(\gamma - \gamma_0) + \frac{\Theta}{\sqrt{3}}(T - T_0) + \frac{\Omega(\xi)}{\sqrt{3}}(\xi - \xi_0)$$

with shear stress τ , shear modulus G , shear strain γ , coefficient of thermal expansion Θ , SMA temperature T , phase transformation coefficient Ω , and martensite fraction ξ . As in [30], we assumed the change due to thermal expansion is negligible. To simplify further, we also assumed the change in strain is negligible, the phase transformation coefficient is constant, and the volume fraction of the Martensite phase in the SMA wire is proportional to the wire temperature, i.e. $\tau \propto T - T_{amb}$. This yields a linear relationship between the shear stress and wire temperature, which we further assume acts uniformly across joints. Lumping these parameters together into β , we arrive at the following linear relationship between the discretized joint torques and the SMA temperature:

$$\tau = \beta(T - T_{amb})\mathbb{1}_n,$$

where $\mathbb{1}_n$ is a vector of ones of length n and n is the number of joints. Because there are two SMA actuators acting antagonistically, the full actuation torque is a combination of the two:

$$\tau = \beta_r(T_r - T_{amb})\mathbb{1}_n - \beta_l(T_l - T_{amb})\mathbb{1}_n,$$

where the subscript r indicates the right-side actuator (inducing counter-clockwise rotation) and subscript l indicates the left-side actuator. The full model dynamics are depicted in figure 3.

V. MODEL CALIBRATION

In order to identify model coefficients that, in simulation, faithfully reproduce the behavior and response of the true hardware, it was necessary to design calibration procedures to isolate individual parameters so they could be reliably estimated. Some simpler parameters could be derived in a straightforward manner, such as the device mass that was measured on a digital weight scale. Based on this, the mass moments of inertia were estimated using the CAD model of the limb. In the subsequent sections we describe the processes used to identify the remaining unknown model coefficients.

A. Thermal actuator temperature dynamics

In order to identify the three parameters in the actuator temperature dynamics system of ODEs (Eqn. 3 and 4), we generated calibration datasets and fit the parameters in an optimization scheme for each actuator independently. The dataset is generated using a PD controller to stabilize the limb at different bend angles where the bend angle φ and thermocouple temperature V are measured and collected along with the commanded duty cycle D . The true SMA wire temperature T is not directly observed, but because we assumed a linear relationship between the temperature and the discretized joint torque we can directly use the bend angle as a proxy for temperature. The scale is calibrated by assuming that, when stabilized, the thermocouple temperature approximately matches the actuator temperature. We used the `DiffEqParamEstim.jl` and `DifferentialEquations.jl`[32] Julia packages to fit the parameters using the two-stage collocation method to find a good initial guess, followed by a least squares optimization to refine the parameters.

B. Torsional spring coefficients

To calibrate the spring coefficient k we oriented the limb with the bending axis parallel to ground and measured the total deflection in static equilibrium under gravitation loading. Under these conditions the equations of motion of the model (equation 2) simplify to 5 and pick up a new term due to gravity, where the spring constant k is the only unknown:

$$k\theta + \tau_g(\theta) = 0. \quad (5)$$

We computed the gravitational loading by taking the gradient with respect to the joint angles of the potential energy of the link centers of mass[33]:

$$\mathbf{r}_i(\theta) = \left(\prod_{j=1}^i e^{\hat{\xi}_j \theta_j} \right) \mathbf{g}_{sl_i}(0) \vec{0} \quad (6)$$

$$U_g(\theta) = mg \sum_{i=1}^n \mathbf{r}_i(\theta) \cdot \mathbf{E}_1 \quad (7)$$

$$\tau_g(\theta) = -\nabla_{\theta} U_g(\theta).$$

where \mathbf{r}_i is the position of the center of mass of link i , $\hat{\xi}_j$ is the twist for joint j , \mathbf{g}_{sl_i} is the mapping from the body frame to the i th center of mass in neutral position ($\theta_i = 0 \ \forall i$), $\vec{0}$ is the zero vector in homogeneous coordinates, U_g is the gravitational potential energy of the system, m is the link mass, g is the force of gravity oriented along the \mathbf{E}_1 axis in the rotated frame, and τ_g is a vector of joint torques due to gravity. When solving for the unknown spring constant k , we don't empirically measure the joint angles θ but instead estimate them using the measured bend angle φ obtained by relating the system to an Euler-Bernoulli beam under gravitational loading. For this estimate, we assume that the curvature decays exponentially moving away from the fixed end such that

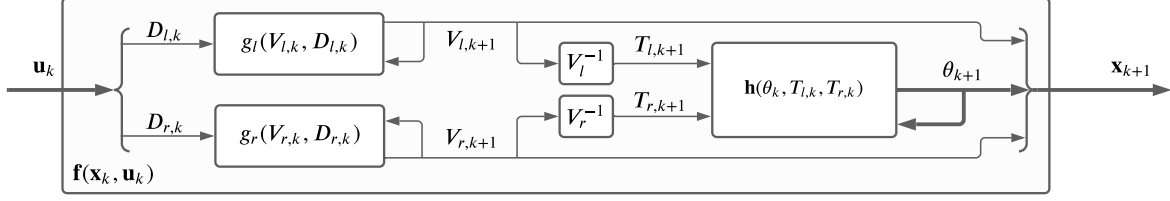


Fig. 3: The full dynamics block f is composed of two actuator dynamics blocks g_l and g_r along with one serial manipulator dynamics block h . Thick arrows and bold letters indicate vectors.

$$\theta_i = \gamma \varphi \frac{(N-i+1)^2}{\sum_{j=1}^N (N-j)^2}$$

where the correction factor $\gamma = 1.22109$ was computed from the model parameters. Then a least-squares fit for k can be computed as:

$$k = -\theta \setminus \mathbf{g}(\theta)$$

C. Actuator force coefficients

To calibrate the actuator force coefficients, we used a PD controller to stabilize the limb at a non-zero bend angle. At static equilibrium, the limb equations of motion simplify to

$$k\theta = \beta(T - T_{amb})\mathbf{1}_n.$$

Since we only measure the bend angle φ we need a mapping to the individual joint angles. We can assume the joint angles are identical and choose them such that the resulting bend angle φ to the tip matches the observed angle. This choice is consistent with the model under static and slow dynamics since we assume identical spring constants and uniform actuation. It can be problematic during rapid motion when the inertial terms are more significant; however, this is not a concern for the case of static equilibrium. Under this assumption the individual joint angles θ_i should be

$$\theta_i = \frac{2\varphi}{n+1}.$$

Now the only unknown is the actuation coefficient β . We can stack the m observations in the dataset into vector $\mathbf{\Gamma}$

$$\mathbf{\Gamma} = \begin{bmatrix} \frac{k}{T_1 - T_{amb}} \theta_1 \\ \vdots \\ \frac{k}{T_m - T_{amb}} \theta_m \end{bmatrix}.$$

Lastly, we can get a least-squares fit to β :

$$\beta = \mathbf{1}_{nm} \setminus \mathbf{\Gamma}.$$

D. Damping coefficient

To calibrate the damping coefficient, we displaced the tip of the limb to 45° , released, and collected data during passive oscillation until the limb came to rest. With no actuation or external loading, the limb equations of motion simplify to 8, where the damping coefficient σ is the only unknown:

$$\mathbf{M}(\theta)\ddot{\theta} + \mathbf{C}(\theta, \dot{\theta})\dot{\theta} + k\theta + \sigma\dot{\theta} = \mathbf{0}. \quad (8)$$

As we only measure the bend angle φ , we would need a mapping to the individual joint angles. Unfortunately, the uniform angle approximation used to calibrate the actuator force coefficients is not valid for the large dynamics in the passive oscillation. There is not a convenient way to measure or derive the joint angles given just the measured bend angle trajectory. However, we can fit a damped sinusoid to the trajectory to recover a damping coefficient:

$$Ae^{-\zeta\omega_n t} \sin(\omega_n \sqrt{1-\zeta^2}t + \phi) + b$$

with magnitude A , damping coefficient ζ , natural frequency ω_n , phase offset ϕ , and bias b . The parameters were fit through constrained optimization to minimize the squared error between the measured data and the reconstructed sinusoid with simple box constraints to speed up convergence.

Taking $\sigma = \zeta\omega_n$ is a reasonable approximation for the damping coefficient of the model, but using it directly tends to add too much damping as it does not exactly correspond to the damping on the individual joint velocities. To fix this we optimize over possible model damping coefficients by minimizing the squared error between the damping coefficient measured from data and the observed tip damping coefficient. This requires rolling out the dynamics with the new coefficient at each iteration, mapping the joint angles to a single tip bend angle, then again fitting a damped sinusoid to recover the damping coefficient.

With all parameters identified, the final model dynamics can be compared to the hardware. Comparisons of the calibrated model and measurements obtained from the hardware testbed are presented in Fig. 4.

VI. TRAJECTORY OPTIMIZATION

Trajectory optimization for the open-loop controls was performed offline using direct collocation. We define the state

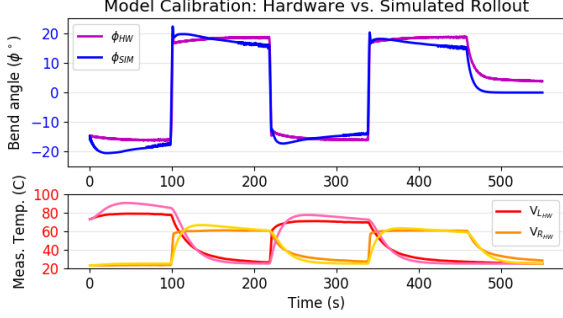


Fig. 4: A test of the calibrated model against hardware data demonstrates close alignment. Temperature simulated rollouts (bottom) in lighter corresponding colors.

vector at time k , \mathbf{x}_k , with the joint angles $\boldsymbol{\theta}$, measured wire temperatures V_l and V_r , and their derivatives. The input vector \mathbf{u}_k contains PWM duty cycles for the left and right actuators:

$$\mathbf{x} = [\boldsymbol{\theta} \quad V_l \quad V_r \quad \dot{\boldsymbol{\theta}} \quad \dot{V}_l \quad \dot{V}_r]^\top, \quad \mathbf{u} = [D_l \quad D_r]^\top \quad (9)$$

We defined a quadratic-cost objective (eqn. 10) subject to constraints (eqns. 11-15) over the entire sequence and used IPOPT [34] to solve the resulting non-linear program (NLP):

$$\arg \min_{\mathbf{x}, \mathbf{u}} \quad \frac{1}{2} \tilde{\mathbf{x}}_N^\top \mathbf{Q}_N \tilde{\mathbf{x}}_N + \frac{1}{2} \sum_{k=1}^{N-1} \tilde{\mathbf{x}}_k^\top \mathbf{Q} \tilde{\mathbf{x}}_k + \mathbf{u}_k^\top \mathbf{R} \mathbf{u}_k \quad (10)$$

$$\text{s.t.} \quad \mathbf{x}_1 = \mathbf{x}_{\text{init}} \quad (11)$$

$$\mathbf{x}_{k+1} = \mathbf{f}(\mathbf{x}_k, \mathbf{u}_k) \quad (12)$$

$$0 \leq u \leq 1 \quad (13)$$

$$T < 100^\circ\text{C} \quad (14)$$

$$T > 45^\circ\text{C} \quad \forall t > 20. \quad (15)$$

Here, N is the number of knot points, $\tilde{\mathbf{x}}_k = \mathbf{x}_k - \mathbf{x}_{k,\text{ref}}$ is the deviation from the reference state at discrete time k , \mathbf{u} is the control input, \mathbf{f} is the discrete dynamics function aggregated from the actuator and limb dynamics as indicated in figure 3, \mathbf{Q} holds the state error penalties, and \mathbf{R} holds the control penalties. Note that the dynamics and optimization are expressed in the joint space, not the task space. To determine the bend angle φ , the exponential map can be used to compute the tip position \mathbf{t} , as in eqn. 6. Then the bend angle can be computed as

$$\varphi = \arctan \left(\frac{\mathbf{t} \cdot \mathbf{E}_2}{\mathbf{t} \cdot \mathbf{E}_1} \right)$$

This is how the tip angle of the optimized trajectory $\bar{\varphi}$ is computed in the results. Note also that, while not part of the state vector, the wire temperature can be derived from eqn. 4 to get $T = V - \dot{V}/a_3$ for each actuator.

An equality constraint (11) is used to specify the known initial configuration. The final configuration is not constrained to simplify convergence and avoid specifying an infeasible

constraint; instead, a large cost \mathbf{Q}_N is specified on the final knot point. Eqn. 12 enforces the dynamics constraints. The control inputs u_k are specified to be between zero and one (13), the physical limits of specifying a pulse width modulation (PWM) duty cycle. Temperature is constrained below a maximum threshold (14) to avoid permanent breakdown of the actuator. Finally, temperature after a warm-up period is constrained to be above 45°C , where the actuator force mapping is reasonably linear.

Figure 5 presents the two trajectories optimized for open-loop control. Both were initialized only by providing the optimizer with a desired tip path (dashed lines). The optimizer then found a solution to the specified NLP.

VII. RESULTS

Open-loop control using the optimized trajectories was performed in hardware, five times each. Mean trajectory and standard deviation bounds are plotted in Fig. 6. Both trajectories show tight run-to-run consistency in tracking the desired bend angle with a deviation under 2.5° between replays 90% of the time. We were able to control the tip to within 10.5° from the reference input for 90% of the time, accumulating considerable deviation in the low-temperature scenarios. The resulting motions in hardware align with the model particularly well in regions of higher temperatures and larger temperature differences.

Both trajectories achieve a largely faithful reproduction of the desired motion, even in open loop, despite simplistic approximations of our soft limb and thermal actuators. The most significant deviations occurred during more aggressive maneuvers where modelling errors were amplified. Deviations were also observed in low-temperature regimes.

VIII. DISCUSSION & CONCLUSION

There are two main sources of error in our model and tests, corresponding primarily to the actuator model. First, the map from PWM duty cycle to observed temperature appears much more dynamic in the hardware than in the simulation. Since our model fits a simple first-order heat transfer model, results indicate an insufficient fit to regions of more aggressive motion. Second, the motion induced by a particular temperature does not appear linear across the actuation range, and the model is inaccurate at low temperatures. Since it is known that the Martensite phase transition of shape-memory materials absorbs some energy, which our model ignores, incorporating this and other constitutive behaviors into the model would improve low-temperature predictions. However, since our robots likely operate at pre-heated temperatures, and soft robots do not necessarily require precision, these limitations may be acceptable. Additional future work will focus on improvements to the temperature and actuation models so as to capture low-temperature behaviors. Modifications to the calibration procedure may also improve results.

Closed-loop control may also address our model mismatch. Future work will examine the time-varying linear quadratic regulator [35] control approach, as well as iterative learning control [36]. In addition, our model is computationally simple

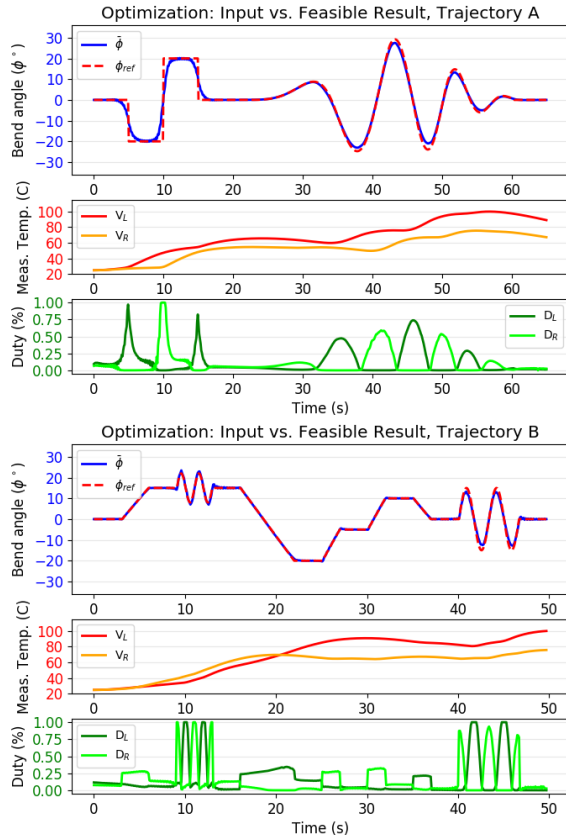


Fig. 5: Two optimized trajectories run in simulation and hardware. Dashed lines represent the desired bend angles, the solid lines represent the trajectory found by the optimizer. PWM duty cycles (as a percent) are the generated inputs.

enough to be directly implemented in resource-constrained hardware, providing opportunity for model-predictive control.

This approach in this article demonstrates the first example of generating and optimizing motion trajectories for soft thermally-actuated robot limbs. Since thermal and shape-memory actuators are some of the simplest to design and fabricate into soft robots, this article provides a platform for computationally generating motions for entirely new categories of robots. Our approach does not require complicated sensor arrays nor computationally-challenging models. Open-loop motions such as these are both simpler to implement, and take advantage of the inherent robustness in soft materials: for certain tasks, it is possible that open-loop operation is all that is needed. Ongoing work seeks to extend our approach to multi-limbed robots, with a goal of generating walking motions of SMA-powered untethered robots (such as [9]).

REFERENCES

- [1] C. Laschi, B. Mazzolai, and M. Cianchetti, “Soft robotics: Technologies and systems pushing the boundaries of robot abilities,” *Science Robotics*, vol. 1, no. 1, p. eaah3690, Dec. 2016.
- [2] C. Majidi, “Soft Robotics: A Perspective - Current Trends and Prospects for the Future,” *Soft Robotics*, vol. 1, no. 1, pp. 5–11, Mar. 2014.
- [3] H. Rodrigue, W. Wang, M.-W. Han, T. J. Kim, and S.-H. Ahn, “An Overview of Shape Memory Alloy-Coupled Actuators and Robots,” *Soft Robotics*, vol. 4, no. 1, pp. 3–15, Mar. 2017.

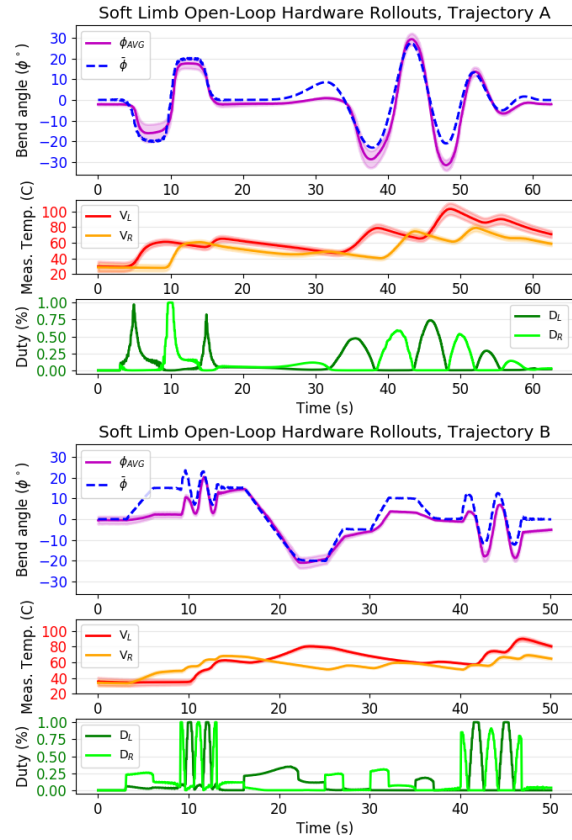


Fig. 6: Open-loop hardware rollouts of the two trajectories optimized in Fig. 5. Solid lines are mean among five trials, shaded regions represent one standard deviation. The model corresponds well to the hardware result after a preheating period, since our approximations are most valid at higher temperatures, as well as in regions of less dynamic behaviors.

- [4] D. Bruder, C. D. Remy, and R. Vasudevan, “Nonlinear System Identification of Soft Robot Dynamics Using Koopman Operator Theory,” in *2019 International Conference on Robotics and Automation (ICRA)*, May 2019, pp. 6244–6250.
- [5] X. Huang, M. Ford, Z. J. Patterson, M. Zarepoor, C. Pan, and C. Majidi, “Shape memory materials for electrically-powered soft machines,” *Journal of Materials Chemistry B*, vol. 8, no. 21, pp. 4539–4551, 2020.
- [6] N. El-Atab, R. B. Mishra, F. Al-Modaf, L. Joharji, A. A. Alsharif, H. Alamoudi, M. Diaz, N. Kaiser, and M. M. Hussain, “Soft actuators for soft robotic applications: a review,” *Advanced Intelligent Systems*, vol. 2, no. 10, p. 2000128, 2020.
- [7] G. Shimoga, T.-H. Kim, and S.-Y. Kim, “An intermetallic niti-based shape memory coil spring for actuator technologies,” *Metals*, vol. 11, no. 8, p. 1212, 2021.
- [8] J. Z. Ge, L. Chang, and N. O. Pérez-Arancibia, “Preisach-model-based position control of a shape-memory alloy linear actuator in the presence of time-varying stress,” *Mechatronics*, vol. 73, p. 102452, Feb. 2021.
- [9] Z. J. Patterson, A. P. Sabelhaus, K. Chin, T. Hellebrekers, and C. Majidi, “An Untethered Brittle Star-Inspired Soft Robot for Closed-Loop Underwater Locomotion,” in *2020 IEEE/RSJ International Conference on Intelligent Robots and Systems (IROS)*, Oct. 2020, pp. 8758–8764.
- [10] A. Doroudchi, R. Khodambashi, M. Sharifzadeh, D. Li, S. Berman, and D. M. Aukes, “Tracking Control of a Miniature 2-DOF Manipulator With Hydrogel Actuators,” *IEEE Robotics and Automation Letters*, vol. 6, no. 3, pp. 4774–4781, July 2021.
- [11] A. T. Luong, H. Moon, H. R. Choi, J. C. Koo, S. Seo, K. Kim, J. Jeon, C. Park, and M. Doh, “Long short term memory model based position-stiffness control of antagonistically driven twisted-coiled

- polymer actuators using model predictive control,” *IEEE Robotics and Automation Letters*, pp. 1–1, 2021.
- [12] M. H. Elahinia and H. Ashrafiuon, “Nonlinear Control of a Shape Memory Alloy Actuated Manipulator,” *Journal of Vibration and Acoustics*, vol. 124, no. 4, pp. 566–575, Oct. 2002.
 - [13] A. D. Marchese, R. Tedrake, and D. Rus, “Dynamics and trajectory optimization for a soft spatial fluidic elastomer manipulator,” *The International Journal of Robotics Research*, vol. 35, no. 8, pp. 1000–1019, July 2016.
 - [14] C. Della Santina, R. K. Katzschmann, A. Bicchi, and D. Rus, “Model-based dynamic feedback control of a planar soft robot: trajectory tracking and interaction with the environment,” *The International Journal of Robotics Research*, vol. 39, no. 4, pp. 490–513, 2020.
 - [15] M. Kelly, “An introduction to trajectory optimization: How to do your own direct collocation,” *SIAM Review*, vol. 59, no. 4, pp. 849–904, 2017.
 - [16] A. P. Sabelhaus, H. Zhao, E. L. Zhu, A. K. Agogino, and A. M. Agogino, “Model-Predictive Control With Inverse Statics Optimization for Tensegrity Spine Robots,” *IEEE Transactions on Control Systems Technology*, vol. 29, no. 1, pp. 263–277, Jan. 2021.
 - [17] W. Huang, X. Huang, C. Majidi, and M. K. Jawed, “Dynamic simulation of articulated soft robots,” *Nature Communications*, vol. 11, no. 1, pp. 1–9, 2020.
 - [18] C. S. Haines, M. D. Lima, N. Li, G. M. Spinks, J. Foroughi, J. D. Madden, S. H. Kim, S. Fang, M. J. De Andrade, F. Göktepe, *et al.*, “Artificial muscles from fishing line and sewing thread,” *Science*, vol. 343, no. 6173, pp. 868–872, 2014.
 - [19] C. Majidi, “Soft-matter engineering for soft robotics,” *Advanced Materials Technologies*, vol. 4, no. 2, p. 1800477, 2019.
 - [20] M. A. Graule, C. B. Teeple, T. P. McCarthy, G. R. Kim, R. C. St. Louis, and R. J. Wood, “Somo: Fast and accurate simulations of continuum robots in complex environments,” in *2021 IEEE International Conference on Intelligent Robots and Systems (IROS)*, 2021.
 - [21] J. Bern, P. Banzet, R. Poranne, and S. Coros, “Trajectory Optimization for Cable-Driven Soft Robot Locomotion,” in *Proceedings of Robotics: Science and Systems*, 2019.
 - [22] A. P. Sabelhaus and C. Majidi, “Gaussian process dynamics models for soft robots with shape memory actuators,” in *2021 IEEE 4th International Conference on Soft Robotics (RoboSoft)*. IEEE, 2021, pp. 191–198.
 - [23] M. Mollaei and S. Mascaro, “Optimal control of multi-input sma actuator arrays on a trajectory using graph theory: Modified a-star search algorithm,” in *Dynamic Systems and Control Conference*, vol. 45301. American Society of Mechanical Engineers, 2012, pp. 743–750.
 - [24] R. Katoch and J. Ueda, “Trajectory planning for antagonistic nonlinearly quantized sma actuator arrays based on evolutionary optimization,” in *2015 American Control Conference (ACC)*. IEEE, 2015, pp. 2631–2636.
 - [25] R. Bena, X.-T. Nguyen, A. A. Calderon, A. Rigo, and N. O. Perez-Arancibia, “Smarti: A 60-mg steerable robot driven by high-frequency shape memory alloy actuation,” *IEEE Robotics and Automation Letters*, 2021.
 - [26] S. H. Sadati, S. E. Naghibi, A. Shiva, I. D. Walker, K. Althoefer, and T. Nanayakkara, “Mechanics of continuum manipulators, a comparative study of five methods with experiments,” in *Annual Conference Towards Autonomous Robotic Systems*. Springer, 2017, pp. 686–702.
 - [27] M. Bergou, M. Wardetzky, S. Robinson, B. Audoly, and E. Grinspun, “Discrete elastic rods,” in *ACM SIGGRAPH 2008 papers*, 2008, pp. 1–12.
 - [28] N. N. Goldberg, X. Huang, C. Majidi, A. Novelia, O. M. O’Reilly, D. A. Paley, and W. L. Scott, “On planar discrete elastic rod models for the locomotion of soft robots,” *Soft robotics*, vol. 6, no. 5, pp. 595–610, 2019.
 - [29] R. J. Webster III and B. A. Jones, “Design and kinematic modeling of constant curvature continuum robots: A review,” *The International Journal of Robotics Research*, vol. 29, no. 13, pp. 1661–1683, 2010.
 - [30] S. S. Cheng, Y. Kim, and J. P. Desai, “Modeling and characterization of shape memory alloy springs with water cooling strategy in a neuro-surgical robot,” *Journal of Intelligent Material Systems and Structures*, vol. 28, no. 16, pp. 2167–2183, 2017.
 - [31] H. Bhargaw, M. Ahmed, and P. Sinha, “Thermo-electric behaviour of niti shape memory alloy,” *Transactions of Nonferrous Metals Society of China*, vol. 23, no. 8, pp. 2329–2335, 2013.
 - [32] C. Rackauckas and Q. Nie, “DifferentialEquations.jl—a performant and feature-rich ecosystem for solving differential equations in julia,” *Journal of Open Research Software*, vol. 5, no. 1, 2017.
 - [33] R. M. Murray, Z. Li, S. S. Sastry, and S. S. Sastry, *A mathematical introduction to robotic manipulation*. CRC press, 1994.
 - [34] A. Wächter and L. T. Biegler, “On the implementation of an interior-point filter line-search algorithm for large-scale nonlinear programming,” *Mathematical Programming*, vol. 106, no. 1, pp. 25–57, 2006.
 - [35] A. Bemporad, M. Morari, V. Dua, and E. N. Pistikopoulos, “The explicit linear quadratic regulator for constrained systems,” *Automatica*, vol. 38, no. 1, pp. 3–20, 2002.
 - [36] A. Schöllig and R. D’Andrea, “Optimization-based iterative learning control for trajectory tracking,” in *2009 European Control Conference (ECC)*. IEEE, 2009, pp. 1505–1510.